Electron transfer rates and Franck-Condon factors: an application to the early electron transfer steps in photosynthetic reaction centers

Borrelli, R.; Di Donato, M.; Peluso, A.

document version
Publisher's PDF, also known as Version of record

REGULAR ARTICLE

Electron transfer rates and Franck–Condon factors: an application to the early electron transfer steps in photosynthetic reaction centers

Raffaele Borrelli · Mariangela Di Donato · Andrea Peluso

Abstract Mechanistic aspects of some of the early electron transfer steps occurring in photosynthetic reaction centers are discussed. Starting from the normal modes of the redox cofactors involved in the electron transfer processes, we show how a series of quantities which regulate electron transfer rates, such as (i) the electron transfer active modes, (ii) the intramolecular reorganization energy, and (iii) the mutual couplings between the vibronic states of the donor and the acceptor, can be obtained and used to draw qualitative conclusions on ET rates.

Keywords Electron transfer · Photosynthesis · Reaction center · Franck–Condon · Duschinsky transformation · Radiationless transition

Introduction

Photosynthetic reaction centers (PRC) are probably the natural energy transducers whose structures and operational properties have been best characterized. The resolution of their crystal structure provided already in the 1980s [1–5] the essential structural information for understanding the structure–function relationships governing energy conversion in photosynthesis. The PRCs are highly spatially organized molecular assemblies contained into a membrane; a schematic view of the cofactors contained in one of such centers (from *Rhodobacter sphaeroides*) is shown in Fig. 1. A bacteriochlorophyll dimer, known as special pair (P), is located at the top of the membrane; a sequence of molecular cofactors arranged on two nearly symmetric branches starts from the special pair. Each branch contains a bacteriochlorophyll (BChl), a bacteriopheophytin (BPh) and a Ubiquinone (UQ) unit. Both branches end at a common nonheme high-spin Fe^{2+} ion surrounded by four neutral histidine residues and a glutamic anion.

The special pair of a PRC functions as a trap for the radiation energy absorbed by the antenna system, for its first excited state lies slightly below those of the chlorophylls located in the antenna system. Radiation energy is then converted into internal energy by promoting a sequence of photoinduced electron transfers (ET), occurring along one of the two branches, which leads to a long-lived charge separated state $P^+Q_A^-$. The resulting electric field then causes protons to be transferred through the membrane so that an electrochemical gradient is established across it, which, according to Mitchell's mechanism, triggers the chemical reactions by which ATP and other biological fuels are produced [6].

In this paper we shall briefly discuss the dynamical features of the early electron transfer (ET) processes occurring in PRCs, with special regard to the role that the chemical structures of the different cofactors and therefore their intramolecular vibrations play in ET, a topic which has been the object of several studies by our group.

From the experimental side, a wealth of data on the rates and relative energies of the ET processes in PRCs are now available, thanks to the constant improvement in spectroscopical time-resolved techniques [7–10]. These advances have allowed for understanding many mechanistic details of the ET steps which ensure the high efficiency of energy conversion in photosynthetic

R. Borrelli · M. Di Donato · A. Peluso (✉)
Dipartimento di Chimica, Università di Salerno,
84081 Baronissi, Salerno, Italy
e-mail: apeluso@unisa.it
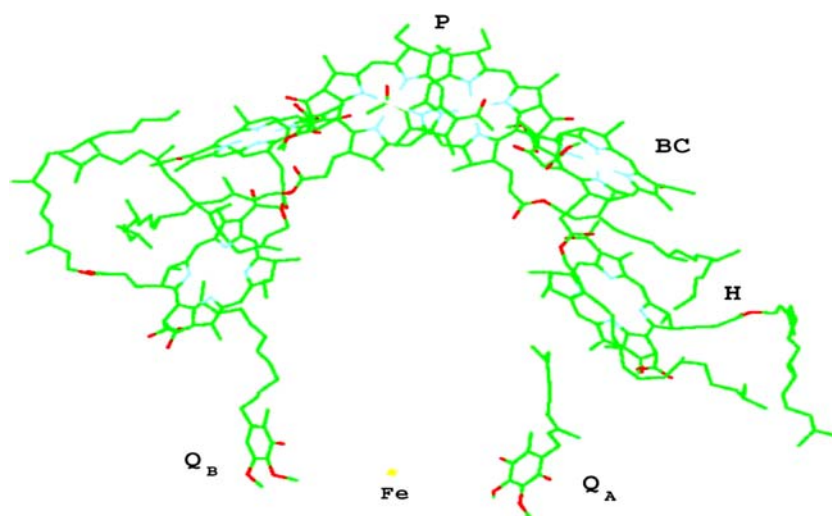
centers. The structural complexity of the PRCs suggests
that high efficiency of energy-conversion should result
from the *coherent* interplay of several structural effects.
A better understanding of that interplay is desirable not
only for scientific purposes but also for technological
progress, particularly in the area of nanostructure re-
search, e.g. in the case of molecular machines capable of
performing similar operations [11–15], whose efficiency
still lies far below that of biosystems.

In the case of photosynthesis, the high efficiency of the
energy conversion is probably connected with the high
stability of the intermediate charge separated state; the
latter requires that a number of energetic and kinetic
requirements should be satisfied.

i. Electron transfer steps have to be fast enough to
    be competitive with respect to radiative or nonra-
    diative decay to the ground state;
ii. Forward electron transfer leading to the final
    charge separated state should be faster than ei-
    ther charge recombination or possible secondary
    processes taking place after each electron transfer
    step;
iii. There should be a low probability of direct,
    "through space" charge recombination from the
    final acceptor to the primary donor, which should
    be far enough and/or separated by a proper shield-
    ing medium.

The most efficient way for the system to fulfill the
above requirements appears to be achieved by an elec-
tron transfer chain in which the primary donor and the
final acceptor are separated by a certain number of
cofactors whose distances and orientations along the
chain allow sequential electron transfer. A closer look

at the kinetics of the ET steps in PRCs also reveals that
the rates of the successive forward ET steps decrease
on approaching the final acceptor: in photosynthetic
PRCs the first photoinduced ET has to be ultrafast in
order to compete with deactivation processes, whereas
the slower rates of the subsequent ET steps allow the
acceptor molecule and its surroundings to relax, mak-
ing back transfer energetically unfavorable. Chlorophyll
and related macrocycles are used in faster ET steps,
whereas quinones are involved in the slower ET steps.
The differences between these two classes of molecules
which could be significant for explaining kinetic data
are:

• Their geometrical changes upon ET;
• The densities and widths of their vibronic bands,
  which must be such that resonance conditions are
  fulfilled in the proper donor–acceptor pairs.

As is well known, two general conditions for ET to
take place are that there should be two quasi-degenerate
states, one belonging to the neutral complex AD and
other to the separated-charge A^-D^+, and that they
are coupled to each other. In the case of ultrafast ET
processes, it is expected that the intramolecular vibra-
tions of the donor and acceptor molecules provide a
sufficiently high density of coupled vibronic states. In
the case of low vibrational-state densities the solvent
modes have to fill up the energy gap between the donor
and the acceptor vibronic states, and the ET rates are
expected to decrease. In the past, a single intramolec-
ular mode coupled to a continuum provided by the
modes of a thermal bath (the surrounding medium)
served as the reference model for the effect of intra-
molecular vibrations in ET dynamics [16,17], but there

are reasons to believe that, although fluctuations introduced by the pertinent interactions of the main ET cofactors with the environment are certainly important for ET, such a simplified model overestimated the role of the bath.

Clearly, the possibility to build more satisfactory models depends on the availability of a detailed analysis of the energies and mutual couplings of the vibronic states of A and of D in both their neutral and charged forms. This paper is mainly intended to show how such an analysis can be conveniently carried out by starting from the knowledge of the normal modes and the vibrational frequencies of the redox cofactors. These data allow the determination of some of the most important parameters for the analysis of ET rates, namely, (i) the intramolecular modes involved in the ET path, (ii) the intramolecular reorganization energy, and (iii) the Franck–Condon weighted density of states of the redox cofactors. This is, to our opinion, the first necessary step toward a proper theoretical modeling of ET dynamics, which of course also requires to take into account the effects of the medium in which the cofactors are embedded, and the relaxation processes which occur after ET. Notwithstanding, the quantities cited earlier, even though computed for the isolated cofactors in the gas phase, allow to extract useful information on ET dynamics and, in the specific case of PRCs, to understand on a molecular basis the reasons for the large ET rate differences observed in the different steps of the photocycle, which spans from picoseconds to microseconds.

Theoretical framework

The reference model we have used in the past for ET in PRCs [18] can be illustrated by the limit case of only two partner molecules, A and D, with a single additional electron. Thus, all the states of the system can be grouped into two subsets, globally denoted by $\overline{|A-D\rangle} \equiv \overline{|A\rangle}$ and $\overline{|AD^-\rangle} \equiv \overline{|D\rangle}$, which are assumed to form a complete and linearly independent basis for ET between A and D.

Any state of the system can then be written as a linear combination of the kets or wavefunctions representing the elements of the two state manifolds:

$$|\Psi(t)\rangle = \overline{|A\rangle}\mathbf{C}_A(t) + \overline{|D\rangle}\mathbf{C}_D(t), \tag{1}$$

where $\mathbf{C}_A$ and $\mathbf{C}_D$ are column vectors, whose sizes are given by the dimensions of the vibrational subspaces of $\overline{|A\rangle}$ and $\overline{|D\rangle}$ considered relevant to the problem under consideration.

The expansion coefficients $\mathbf{C}(t)$ of Eq. (1) determine the time evolution of $|\Psi(t)\rangle$ and therefore the dynamics of ET; they are solutions of the time dependent Schrödinger equation:

$$-i\hbar \begin{pmatrix} \dot{\mathbf{C}}_A(t) \\ \dot{\mathbf{C}}_D(t) \end{pmatrix} = \begin{pmatrix} \mathbf{H}_{AA} & \mathbf{H}_{AD} \\ \mathbf{H}_{AD}^\dagger & \mathbf{H}_{DD} \end{pmatrix} \begin{pmatrix} \mathbf{C}_A \\ \mathbf{C}_D \end{pmatrix}, \tag{2}$$

with initial conditions specifying the initial state of the system. Each of the four matrix blocks in Eq. (2) is a matrix whose size depends on the number of vibrational states belonging to $\overline{|A\rangle}$ and $\overline{|D\rangle}$. Since its off-diagonal elements are in general nonvanishing, the elements of $\overline{|A\rangle}$ and $\overline{|D\rangle}$ are not eigenstates of the Hamiltonian operator and change in time.

In the Born–Oppenheimer approximation:

$$|A\bar{v}\rangle = |\psi_A\rangle \otimes |\bar{v}_A\rangle, \quad |D\bar{w}\rangle = |\psi_D\rangle \otimes |\bar{w}_D\rangle, \tag{3}$$

where $\bar{v}$ and $\bar{w}$ denote the whole set of the vibrational quantum numbers associated to the ET active normal modes of vibration, the matrix elements of the diagonal and extradiagonal blocks of H are:

$$H_{A\bar{w}A\bar{v}} = \langle A\bar{v}| \mathcal{H}^{el} + \mathcal{T}_N |A\bar{w}\rangle$$
$$= \langle \bar{v}_A| \mathcal{E}_A(R) + \mathcal{T}_N |\bar{w}_A\rangle = E_{A\bar{v}}^{tot} \delta_{\bar{w},\bar{v}} \tag{4}$$

$$H_{A\bar{w}D\bar{v}} = \langle A\bar{v}| \mathcal{H}^{el} + \mathcal{T}_N |D\bar{w}\rangle$$
$$= \langle \bar{v}_A| \lambda(R) + \langle A| \mathcal{T}_N |D\rangle |\bar{w}_D\rangle, \tag{5}$$

where $\mathcal{E}_A(r)$ is the nuclear potential energy operator of $\overline{|A\rangle}$ and:

$$\lambda(R) = \langle A| \mathcal{H}^{el} |D\rangle. \tag{6}$$

The extradiagonal terms can be further simplified by making the reasonable assumption that:

$$\lambda(R) >> \langle A| \mathcal{T}_N |D\rangle. \tag{7}$$

By further neglecting the dependence of $\lambda(R)$ on the nuclear coordinates, we arrive at the well-known result that the off-diagonal terms are proportional to the overlap of the vibrational states of $|A\rangle$ and $|D\rangle$, the so-called Franck–Condon integrals:

$$H_{A\bar{w}D\bar{v}} = \lambda \langle \bar{v}_A|\bar{w}_D\rangle. \tag{8}$$

The ingredients essential for building a reasonably approximate form of the Hamiltonian matrix which determines the time evolution of the (A,D) system are therefore:

i.   The relative energy of the two electronic states;
ii. The electronic coupling term λ;

iii. The vibrational frequencies and the normal modes of vibrations of the two electronic states;

iv. The Franck–Condon integrals.

The relative energy of the two electronic states (including the zero point contribution) can be obtained by spectroscopic measurements [9,19,20], and the electronic coupling term can be reliably estimated by using empirical expressions [21].

Concerning the normal modes of vibrations, which imply the knowledge of the minimum energy geometries of A^-D and AD^-, highly reliable estimates are necessary because both these factors play an important role in ET. In some of our applications these quantities have been therefore obtained by high level ab initio computations for the isolated molecules in their neutral and anionic forms [18]. In this way accurate estimates of geometrical changes upon ET and of normal modes are obtained, but the possible effect of the surrounding medium and of the intermolecular modes is ignored. In weakly coupled systems, such as PRCs, the couplings between the vibronic states of $\overline{|A\rangle}$ and $\overline{|D\rangle}$ are dominated by the displacements of the equilibrium positions of the normal and reduced forms of the redox cofactors rather than by frequency changes or normal mode mixing. The equilibrium displacements are rather unaffected by the interaction with the protein matrix, and therefore the effect of the environment is mainly that of causing small energy fluctuations of the electronic energy difference between the initial and final state, which allows for fulfilling degeneracy conditions. In some cases, as that of ultrafast ET, this effect can be included by making suitable averages of the transition probabilities over a small energy range around the observed value of the electronic energy difference between $\overline{|A\rangle}$ and $\overline{|D\rangle}$ [18]. Such a model turned out to be successfull in the case of ET from pheophytin to ubiquinone in PRCs, probably because the relaxation of the environment takes place on longer timescale than ET, as also suggested by some experimental results [22]. Of course, there are cases where solvent relaxation and ET occur with comparable rate [17], several alternative approaches are available for them [23,24].

Energy fluctuations can be studied by resorting to hybrid quantum mechanic/molecular mechanic approaches; work is in progress along this line.

Finally, a legitimate simplification is the use of the harmonic approximation, because highly excited vibrational states will not play an important role, see infra; the generalization to anharmonic potential poses no problems, but it of course makes computations more demanding.

ET active modes

In the discrete state approach to ET dynamics, the selection of the vibrational states to be used in the time evolution is probably the most important problem. Two factors determine the involvement of a given state in the dynamics of the system: the energy and its couplings with the initial state and with the other states which can be populated in the time evolution of the system. The coupling between two states can be either direct or indirect, i.e. mediated by a third state whose energy can be outside the range in which vibrational states can be effectively populated. Because of the indirect couplings, the criterion purely based on the selection of a small energy range cannot be adopted. Since the density of states of large protein cofactors hugely increases with the energy, the problem would rapidly become unsolvable as the energy difference between the vibronic ground states of the initial and final states increases.

The difficulty posed by indirect couplings is minimized (completely avoided in the case of only two electronic states) by using a basis of oscillators for each electronic state, so that the two diagonal blocks of Eq. (2) are diagonal matrices. More important, the use of such a basis offers the advantage that the most coupled modes can be determined by projecting the normal modes of one electronic state into those of the other: only those modes which are either displaced or mixed with each other for the effect of the change of the electronic potential energies upon ET can change their quantum numbers during the time evolution of the system; all other modes will be frozen in their initial quantum state, because changes in quantum numbers would make the Franck–Condon integrals, and therefore the whole coupling with the initial state, vanishingly small, even in the case where the vibrational frequency changes upon the electronic transition.

The displaced and mixed modes can be determined by Duschinsky's transformation [22];

$$\mathbf{Q}_l = \mathbf{J}\mathbf{Q}_m + \mathbf{K}, \tag{9}$$

where $\mathbf{Q}_l$ and $\mathbf{Q}_m$ are the normal mode vectors of the two electronic states $|l\rangle$ and $|m\rangle$, $\mathbf{J}$ is the rotation matrix and $\mathbf{K}$ the displacement vector.

The rotation matrix $\mathbf{J}$ and the displacement vector $\mathbf{K}$ can be easily determined once the equilibrium geometries and the normal modes of the two electronic states are known [23]. If the normal modes of the two electronic states are expressed in terms of Cartesian coordinates $\boldsymbol{\xi}$ of the nuclei:

$$\boldsymbol{\xi} - \boldsymbol{\xi}_1^0 = \mathbf{L}_1\mathbf{Q}_1 \quad \boldsymbol{\xi} - \boldsymbol{\xi}_2^0 = \mathbf{L}_2\mathbf{Q}_2, \tag{10}$$

where $\boldsymbol{\xi}_i^0$ and $\boldsymbol{\xi}_f^0$ are the equilibrium nuclear coordinates of the two electronic states, and $\mathbf{L}_i$ and $\mathbf{L}_f$ are the rectangular matrices of the normal modes, the rotation matrix and the displacement vector of Eq. (9) are given by:

$$\mathbf{J} = \mathbf{L}_1^\dagger \mathbf{S} \mathbf{L}_2 \quad \mathbf{K} = \mathbf{L}_1^\dagger (\mathbf{S}\boldsymbol{\xi}_2^0 - \boldsymbol{\xi}_1^0) \tag{11}$$

The $\mathbf{S}$ matrix accounts for the so-called zero-order axis-switching effect in the normal mode transformation [24].

Duschinsky's transformation is also the starting point for evaluating multi-dimensional Franck–Condon integrals; there are several procedures in the literature to compute Franck–Condon integrals [25,26], we have used that of reference [25], implemented in the computer program MOLFC [27].

The most significant components of the $\mathbf{K}$ vector and coefficients of the $\mathbf{J}$ matrix for the pairs BChl/BChl⁻, BPh/BPh⁻, and UQ/UQ⁻ are reported in Tables 1, 2 and 3, respectively.

All the ET cofactors possess several modes whose equilibrium positions are significantly displaced upon ET, covering a wide range of wavenumbers, from 25 to $1,800$ cm⁻¹. The high frequency modes are very important because they make the filling up of a large electronic energy gap possible between the initial and final states with a modest increase in vibrational quantum numbers. The low-frequency modes are important for fine-energy tuning, i.e. for achieving the tight degeneracy between initial and final vibronic states, which is necessary for tunneling [18].

UQ/UQ⁻ pair differs somewhat from the others because of the higher number of significantly displaced modes and because the modes with larger displacements fall at higher energy than those of BChl and BPh. These features make quinones particularly suited for ET between states with a large electronic energy difference, whereas BChl and BPh, whose most displaced modes fall at very low wavenumbers, appear to be well suited for ET between quasi-degenerate electronic state. For the same reasons the intramolecular reorganization energy of UQ/UQ⁻ is expected to be much higher than those of BChl and BPh.

As to the Duschinsky effect, there are important differences between the three pairs. In UQ/UQ⁻ and BChl/BChl⁻ there are two groups of significantly mixed modes, one including the lowest frequency modes, the other the highest frequency modes. By contrast, BPh exhibits a large number of mixed modes, in a wide region of wavenumbers, which can be grouped into four subsets. The first group includes the five lowest frequency modes, the second one consists of 12 modes spanning the region from 794 to 886 cm⁻¹, cf. Table 2, the last two groups include 8 modes, from 1,088 and 1,191 cm⁻¹, and 13 modes, falling in the wavenumber range 1,327–1,509 cm⁻¹.

Reorganization energies

Intramolecular reorganization energies (ϵ) can be easily computed from the displacement vector of Eq. (11); in harmonic approximation:

$$\epsilon = \frac{1}{2} \sum_i \hbar\omega_i K_i^2, \tag{12}$$

Table 1 Progressive normal mode number, wavenumbers (cm⁻¹), dimensionless displacements, and mixing coefficients of the most displaced[a] or mixed[b] normal modes of the pair BChl/BChl⁻. DFT/B3LYP/6-31g computations

Mode	Wavenumber		K	J[a]
	BCl⁻	BCl		
1	19.378	32.496	−0.637	−0.78(1)−0.30(2)−0.42(4)+0.29(5)
3	55.737	62.773	0.805	0.74(2)−0.54(4)+0.28(5)
4	64.909	67.939	−0.357	
6	100.413	101.508	0.314	
8	137.706	141.019	0.249	
13	205.781	206.617	−0.385	
19	310.027	307.505	−0.270	
21	320.782	320.545	0.236	
43	729.671	729.767	0.372	
49	787.439	789.573	0.331	
67	1018.958	1026.857	0.274	
115	1678.682	1690.179	0.437	−0.33(113)+0.32(114)−0.50(115)+0.72(116)
116	1701.425	1723.979	0.378	0.26(113)−0.81(115)−0.49(116)
121	3041.899	3066.626	−0.256	−0.32(120−0.77(122)+0.49(125) +0.16(127)

Most displaced modes: only modes with displacement longer than 0.25; mixed normal modes: only mixed modes with maximum coefficient lower than 0.85
[a] Numbers in parenthesis refer to the modes of BCl

Table 2 Progressive normal mode number, wavenumbers (cm^{-1}), dimensionless displacements, and mixing coefficients of the most displaced or mixed normal modes of the pair BPh$^-$/BPh

| Mode | Frequency | | K | J[a] |
	BPh$^-$	BPh		BPh$^-$ → BPh
1	28.410	32.630	0.001	0.64(1)+0.68(2)+0.16(3)−0.15(4)+0.23(5)−0.15(7)
2	34.450	48.460	0.000	−0.76(1)+0.57(2)+0.11(3)−0.15(4)+0.22(5)
3	57.450	67.360	−0.001	0.40(2)−0.14(3)+0.52(4)−0.73(5)
4	67.440	70.020	0.000	−0.14(2)+0.96(3)−0.20(5)
5	74.340	81.450	−0.004	0.82(4)+0.55(5)
6	94.730	108.980	−0.098	
9	135.380	135.480	0.355	
10	146.600	146.220	0.884	
18	275.980	277.640	0.358	
29	540.440	529.850	0.266	
41	731.900	730.640	0.262	
46	794.930	810.150	−0.250	0.71(47)−0.43(48) 0.52(54)−0.10(57)+0.11(58)
47	805.520	814.750	−0.250	→ 46
48	810.860	834.010	0.000	−0.37(47)−0.44(48)+0.20(50)+0.50(51)+0.18(54)+0.56(55)
49	823.660	839.860	0.018	0.48(47)+0.50(48)+0.43(50)+0.43(51)−0.27(54)+0.21(55)
50	830.850	842.930	0.000	−0.18(47)+0.52(48)−0.15(50)+0.19(51)+0.74(54)−0.23(58)
51	832.020	844.880	0.000	→ 49
52	837.680	863.700	−0.090	0.64(50)−0.59(51)+0.21(54)+0.16(55)+0.20(57)−0.30(60)
53	851.350	865.040	−0.028	0.13(47)+0.19(48)−0.32(50)−0.33(51)+0.73(55)−0.40(57)
54	852.540	867.250	0.000	0.82(52)−0.56(53)
55	857.430	882.850	0.000	−0.55(52)−0.82(53)
57	875.630	904.070	0.000	+0.21(48)+0.14(51)+0.12(54)−0.29(57)+0.88(58)
58	886.480	916.300	0.000	→ 56
78	1184.400	1204.920	−0.248	
101	1454.200	1473.730	−0.268	
114	1654.030	1658.350	0.289	
115	1669.830	1673.170	−0.304	

Normal modes and vibrational frequencies from DFT/B3LYP/3-21g computations; optimum geometries from DFT/B3LYP/6-31g** computations; Most displaced modes: only modes with displacement longer than 0.25; Mixed normal modes: only mixed modes with maximum coefficient lower than 0.85

[a] Numbers in parenthesis refer to the modes of BPh

where K_i is in adimensional units. In Table 4 the intramolecular contributions to the reorganization energy for the three ET steps, BChl → BChl$^-$, BPh → BPh$^-$, and UQ → UQ$^-$, are reported. Intramolecular contributions to ϵ have been calculated in three different ways: (i) from geometry optimizations and energy computations at DFT/B3LYP level of computations, see Tables 1–3 for more details, (ii) by Eq. (12), and (iii) by Eq. (12) but summing only over those modes which have been chosen as active modes for ET in Franck–Condon (FC) calculations; the last method provides an indication about the completeness of the vibrational basis set used in FC computations.

The total intramolecular reorganization energy yielded by DFT/B3LYP computations for ET from BPh to UQ is 0.40 eV, 0.1 coming from BPh and 0.3 from UQ. The total reorganization energy computed by summing over all modes is *ca.* 0.41 eV, about 0.3 eV from UQ and 0.1 eV from BPh, testifying that harmonic approxima-

tion can be safely used both for evaluating FC integrals and for the fitting of important parameters from ET rates.

The most displaced mode of UQ$^-$ (473 cm^{-1}) contributes to half of the whole reorganization energy of UQ$^-$, whereas for BChl and BPh, there are no dominant modes. Almost all the reorganization energy of UQ is associated with modes which are included in FC calculations, whereas the pheophytin modes included in FC computations cover only 40% of its reorganization energy. This is an indication of the importance of numerous slightly displaced modes between 1,400 and 1,700 cm^{-1}, which cannot be all included in our calculations due to current limitations of MOLFC program (actually, MOLFC can handle about 10^6–10^7 FC integrals, so that by factorizing the FC integrals in a product of integrals referring to the acceptor and to the donor group it is possible to compute about 10^{13} FC integrals).

Table 3 Progressive normal mode number, wavenumbers (cm^{-1}), dimensionless displacements, and mixing coefficients of the most displaced or mixed normal modes of the pair Q_A/Q_A^-. DFT/B3LYP/6-31++g** computations

p Mode	Frequency		**K**	**J**[a]
	Q_A	Q_A^-		$Q_A \rightarrow Q_A^-$
1	24.220	76.410	0.313	0.29(1)−0.44(2)+0.75(3)+0.23(5)+0.31(6)
2	42.370	86.160	−0.260	0.83(1)+0.17(2)−0.31(3)+0.41(5)
3	75.060	93.160	−0.018	0.85(2)−0.51(3)
4	89.980	128.060	0.338	0.28(1)+0.83(4)−0.46(5)
5	117.980	149.700	0.176	0.37(1)+0.54(4)+0.75(5)
9	277.930	318.450	0.324	
12	375.150	367.500	−0.572	
13	420.390	420.770	−0.145	0.74(13)+0.64(14)
14	423.840	447.120	−0.151	−0.65(13)+0.74(14)
15	460.290	473.290	1.629	
19	649.670	667.610	0.254	
30	1179.790	1174.460	0.783	
32	1227.580	1220.390	−0.346	
41	1529.680	1521.060	0.461	
45	1723.790	1545.190	0.708	
46	1729.290	1643.850	0.803	
49	3147.930	3074.420	−0.002	−0.72(49)+0.64(50)+0.15(51)−0.16(52)
50	3152.000	3076.300	0.007	0.66(49)+0.73(50)
51	3183.810	3121.070	−0.001	−0.16(49)+0.16(50)−0.65(51)+0.73(52)
52	3187.810	3121.180	−0.002	0.74(51)+0.66(52)

Most displaced modes: only modes with displacement longer than 0.1; Mixed normal modes: only mixed modes with maximum coefficient lower than 0.85

[a] Numbers in parenthesis refer to the modes of Q_A^-

Table 4 Reorganization energies (cm^{-1}) for the BChl$^-$/BPh → BChl/BPh$^-$, BPh$^-$/UQ → BPh/UQ$^-$, and UQ$^-$/UQ → UQ/UQ$^-$ process

A	B	DFT/B3LYP		Harmonic		Excited modes	
		A	B	A	B	A	B
BCl$^-$	Phe	860	1,300	1,148	825	237	272
Phe$^-$	Ubi	834	2,427	830	2,472	269	2,288
Ubi$^-$	Ubi	2,443	2,427	2,420	2,472	2,055	2,288

Franck–Condon integrals

The absolute values of the FC integrals for ET from BChl$^-$ to BPh, from BPh$^-$ to UQ, and finally from the primary to secondary UQ are plotted versus the vibrational energy of the final states in Figs. 2, 3 and 4, respectively. For each case, it has been assumed that ET occurs from the ground vibrational state of each initial state, whose energy has been set to zero. The vibrational modes of the final state which have been excited in the computation of FC integrals and the maximum number of states for each mode are specified in the notes of Figs. 2–4.

The insets of Figs. 2–4 show magnifications over a tiny energy region corresponding to the experimental free energy change upon ET. Since in the model adopted here the coupling between vibronic states are proportional to FC integrals, Figs. 2–4 provide pictures of the

manifolds of vibronic states which can be involved in the three ET processes.

For ET from BChl$^-$ to BPh and from BPh$^-$ to UQ there is a dense manifold of final vibronic states which are weakly coupled to the ground initial vibronic state and a more sparse set of strongly coupled states, cf. Figs. 2 and 3. These results would suggest that, provided that small energy fluctuations, much smaller than a thermal quantum $k_b T$ (k_b Boltzmann constant), take place, ET from BChl$^-$ to BPh and from BPh$^-$ to UQ can be mechanistically modeled as a nonradiative transition which mainly involves the intramolecular modes of vibrations of the two redox cofactors, without the assistance of the low-frequency modes of the medium. This conclusion is in good agreement with the general finding that the rates of most ET processes occurring in photosynthetic reaction centers (P* → BPh, BPh$^-$ →UQ, UQ$^-$ → P$^+$) are only moderately temperature-dependent [28–32].

Fig. 2 Absolute values of the Franck–Condon integrals as a function of the vibrational energy difference for the transition: $\left|BChl^-BPh\right\rangle_{\bar{v}=0} \to \left|BChlBPh^-\right\rangle_v$. Wavenumbers ($cm^{-1}$) and number of states (in parenthesis) for each oscillator of the excited modes: BChl {135.48(3), 146.22(5), 225.01(2), 277.64(2) 297.92(1), 386.37(2), 529.85(2), 659.67(2), 724.18(2), 730.64(2), 761.60(2), 788.83(2), 1281.39(2), 1691.72(2), 1761.78(2)}; BPh {76.41(2), 86.16(1), 128.06(1), 206.90(2), 318.45(1), 367.50(4), 473.29(6), 1000.67(1), 1083.25(1), 1167.06(1), 1174.46(4), 1447.34(2), 1494.19(3), 1545.19(3), 1643.85(1)}
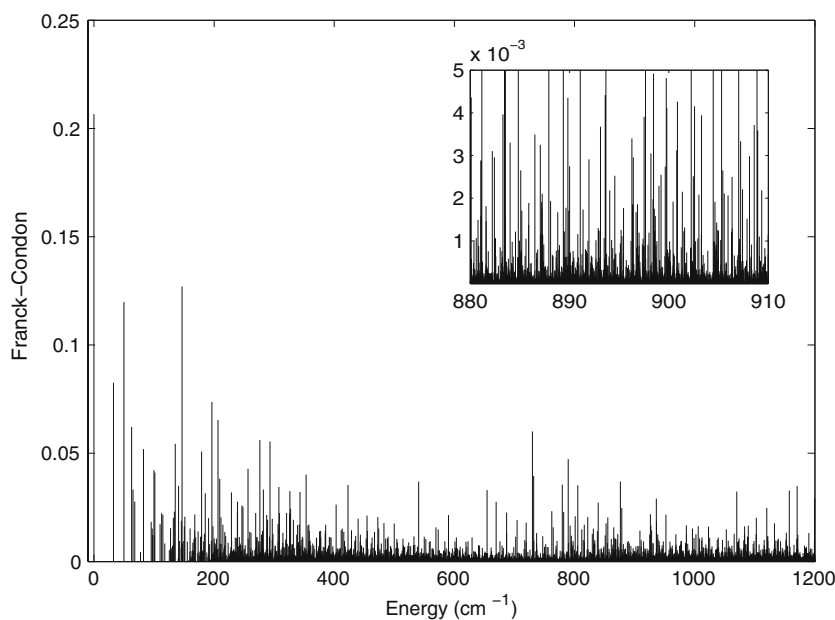

Fig. 3 Absolute values of the Franck–Condon integrals as a function of the vibrational energy difference for the transition: $\left|BPh^-UQ\right\rangle_{\bar{v}=0} \to \left|BPhUQ^-\right\rangle_v$. Wavenumbers ($cm^{-1}$) and number of states (in parenthesis) for each oscillator of the excited modes: BChl {135.48(3), 146.22(5), 225.01(2), 277.64(2) 297.92(1), 386.37(2), 529.85(2), 659.67(2), 724.18(2), 730.64(2), 761.60(2), 788.83(2), 1281.39(2), 1691.72(2), 1761.78(2)}; BPh {76.41(2), 86.16(1), 128.06(1), 206.90(2), 318.45(1), 367.50(4), 473.29(6), 1000.67(1), 1083.25(1), 1167.06(1), 1174.46(4), 1447.34(2), 1494.19(3), 1545.19(3), 1643.85(1)}
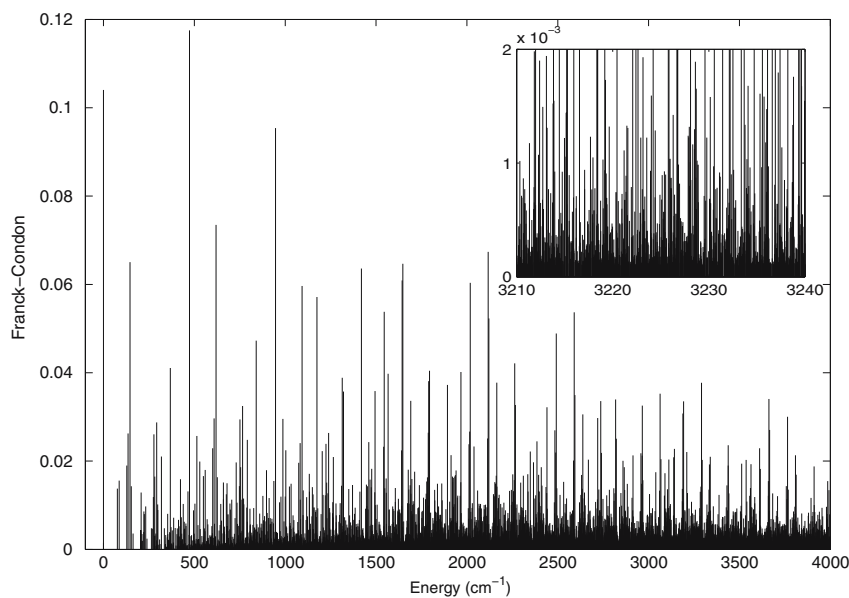

The dynamics of ET from BPh^- to UQ have been successfully examined in a previous paper [18]; by considering only the intramolecular modes of the two moieties we obtained a transition time of ca. 200 ps, in good agreement with experimental results. It is worth noticing that all the intramolecular vibrational degrees of freedom have been explicitly considered, so that the faster contribution to the dephasing has been explicitly included in dynamics. Of course our dynamics are periodic, because the slower dephasing due to the interaction with the environment has been omitted; there are experimental indications suggesting that, in the specific case of photosynthetic systems, this effect is slightly slower than 200 ps [22], so that it should be mainly responsible of the irreversible decay which is not present in our previous simulations.

According to our present results, the most important mode in ET dynamics is that at 473 cm^{-1} of UQ. That is in very good agreement with previous attempts to fit the temperature dependence of ET rates based on the

Fig. 4 Absolute values of the Franck–Condon integrals as a function of the vibrational energy difference for the transition: $\left|UQ_A^- UQ_B\right\rangle_{\bar{v}=0} \rightarrow \left|UQ_A UQ_B^-\right\rangle_v$. Wavenumbers (cm^{-1}) and number of states (in parenthesis) for each oscillator of the excited modes: *a*) BChl {135.48(3), 146.22(5), 225.01(2), 277.64(2) 297.92(1), 386.37(2), 529.85(2), 659.67(2), 724.18(2), 730.64(2), 761.60(2), 788.83(2), 1281.39(2), 1691.72(2), 1761.78(2)}; BPh {76.41(2), 86.16(1), 128.06(1), 206.90(2), 318.45(1), 367.50(4), 473.29(6), 1000.67(1), 1083.25(1), 1167.06(1), 1174.46(4), 1447.34(2), 1494.19(3), 1545.19(3), 1643.85(1)}
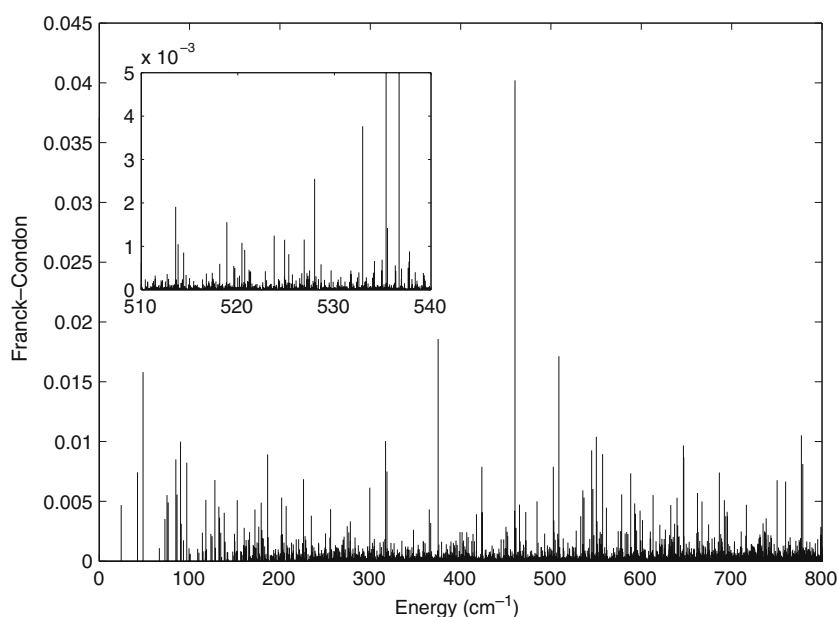
Fermi golden rule and on ad hoc estimates of normal mode displacements and frequencies [33], according to which the simplest and most successful model for ET rate would imply a quantum mode at 400 cm^{-1} and at least two soft modes at low frequency (50 and 10 cm^{-1}). The two soft modes necessary to fit the temperature dependence of ET rates could be provided by the two low frequency vibrations of neutral UQ, falling at 24 and 42 cm^{-1}, which are both significantly displaced to play a role in ET, cf. Table 3. Furthermore, the assumption made by Schenck et al. of a much smaller ΔE_{el} 390 cm^{-1} than that suggested by delayed fluorescence measurements [34] (3,000–5,500 cm^{-1}) is not necessary in our treatment, because ET is significantly coupled also to high frequency modes, both of BPh and of Q_A, which can account for the larger electronic energy difference, as clearly shown by the inset of Fig. 3.

Figures 2 and 3 strongly suggest that ET from BChl$^-$ to BPh should be faster, in agreement with experimental observations; work is in progress along this line.

The slow ET between quinones

Coming to ET between primary and secondary quinones, a very important point is that the $P^+Q_A^-$ state should live long enough for the reduction of P^+ by cytochrome c to occur. The results reported in Fig. 4 suggest that ET between the primary and secondary ubiquinone should be somewhat slower than ET from BPh$^-$ to UQ, but there is evidence, experimental [35,36] as
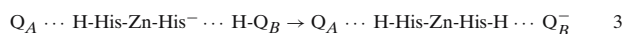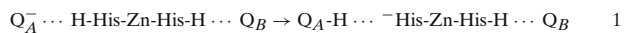
well as theoretical, [37] that other processes take place on a faster timescale, which stabilize the ubiquinone anion thus overcoming the structural conditions used to obtain Fig. 4.

Kinetic studies have provided evidence in favor of a temperature- dependent extra stabilization of the $P^+Q_A^-$ state, which can be either due to solvent reorganization, [35,36] or possibly to some chemical modification at Q_A, probably involving proton movements around Q_A. In line with the latter hypothesis, the Q_A^-/Q_A FTIR difference spectra of photosynthetic RCs, both from *Rb. sphaeroides* and from *Rp. viridis*, show a broad positive band at 2,900–2,500 cm^{-1}, shifting at 2,200–1,800 cm^{-1} upon deuteration [38]. According to previous studies [39,40], such a band has been tentatively assigned to proton vibrations within a network of polarizable H-bonds, thus suggesting that the formation of Q_A^- could cause a significant rearrangement of the H-bond network around Q_A.

Proton transfer (PT) can also be an efficient way to stabilize charge separated states: Hung et al. have shown that, in carotenoid-porphyrin-quinone triads exhibiting photoinduced ET, the addition of a carboxylic group, in a position in which it can form an intramolecular H-bond with a quinone oxygen, significantly stabilizes the charge separated state, probably by transferring a proton from the carboxylic group to the semiquinone anion [41].

Theoretical computations support the hypothesis that the arrival of an electron on Q_A can lead to significant proton rearrangements around Q_A. Semiempirical

MNDO/PM3 as well as unrestricted Hartee–Fock ab initio computations (with the standard 6-31G basis set and polarization functions on the atoms engaged in H-bonds), carried out on a model system of Zn substituted RC consisting of the two quinones and the metal ion with its full coordination sphere, confirm that ET from Q_A to Q_B can occur via the proton assisted electron transfer (PAET) mechanism schematized subsequently [42–44]:

$$Q_A^- \cdots \text{H-His-Zn-His-H} \cdots Q_B \rightarrow Q_A\text{-H} \cdots {}^-\text{His-Zn-His-H} \cdots Q_B \qquad 1$$

$$Q_A\text{-H} \cdots {}^-\text{His-Zn-His-H} \cdots Q_B \rightarrow Q_A \cdots \text{H-His-Zn-His}^- \cdots \text{H-}Q_B \qquad 2$$

$$Q_A \cdots \text{H-His-Zn-His}^- \cdots \text{H-}Q_B \rightarrow Q_A \cdots \text{H-His-Zn-His-H} \cdots Q_B^- \qquad 3$$

Scheme 1

Upon the arrival of an additional electron on Q_A^-, the latter takes up the proton of the H-bonded HisM219, localizing the negative charge of the iron-histidine bridge, step (1). Since the two quinones are chemically equivalent and the driving force for ET is small, being provided by the different environments of Q_A and Q_B [45,46], the nuclear configuration formed after PT is nearly degenerate with that in which Q_B is protonated and the negative charge is localized on HisL190, the iron histidine ligand opposite to HisM219, forming H-bond with Q_B. Thus, the shift of the two H-bonded hydrogens, proton plus electron, carries an electron from Q_A to Q_B (2); Q_A will be back in its initial state, having received an electron and a proton and released a hydrogen atom. Finally, Q_B-H will release a proton to the adjacent histidine, leading to the ET product (3). All the steps involved in the PAET mechanism reported in Scheme 1 are predicted to be slightly exoergic, so that it was concluded that PAET mechanism is energetically plausible and worthy of further experimental investigation [44]. Quantum dynamic simulations of the first PT step, performed on a reliable potential energy surface, obtained by ab-initio computations with full geometry optimization and inclusion of electronic correlation at MP2 level, showed that the PT step is not only exoergic but also very fast, occurring on a timescale of a few tens of fs, much faster than the results of Fig. 4 would predict for direct ET [37]. According to those results, PT from the iron–histidine to the semiquinone anion could be the chemical process which stabilizes the charge separated state, increasing its lifetime.

Final remarks

Efficient energy conversion occurring in natural PRCs is the result of several sequential ET steps which take place with very different mechanisms. Ultrafast ET steps, required at the very beginning of the photoinduced process for avoiding radiative decay to the ground state, can be thought of as radiationless processes mainly involving the intramolecular modes of the redox pairs. Large macrocycles are well suited for ultrafast ET processes, because their vibrational states provide a quasi-continuum of weakly coupled vibronic states. Smaller molecules, such as quinones, are used in the last steps of ET sequence for decreasing ET rates, because of their much lower density of coupled vibronic states. On decreasing ET rates, relaxation processes, necessary to stabilize the final charge separated state, have time to occur. Theoretical analyses suggest that a proton transfer from a histidine residue coordinated to the Fe^{2+} ion could be the leading process for stabilizing the ubiquinone anion. Proton transfer prevents from an easy radiationless decay to the ground state, which, after the sequences of the ET steps took place, is only 0.5–0.6 eV lower in energy than the charge separated state, and makes ET from primary to secondary quinone a much slower step.

References

1. Deisenhofer J, Michel H (1989) EMBO J 8:2149
2. Deisenhofer J, Epp O, Sinning I, Michel H (1995) J Mol Biol 246:429
3. Feher G, Allen JP, Yeats TO, Chirino A, Rees DC, Komiya H (1988) Proc Natl Acad Sci USA 85:7993
4. Feher G, Allen JP, Yeats TO, Chirino A, Rees DC, Komiya H (1988) Proc Natl Acad Sci USA 85:8487
5. Stowell MHB, McPhillips T, Rees DC, Soltis SM, Abresch E, Feher G (1997) Science 276:812–816 PDB ID: 1AIG
6. Mitchell P (1961) Nature (Lond) 191:144–148
7. Wang HY, Lin S, Woodbury NW (2006) J Phys Chem B 110:6956
8. Yakovlev AG, Jones MR, Pottern JA, Fyfe PK, Vasilieva LG, Shkuropatov AY, Shuvalov VA (2005) Chem Phys 319:297–307
9. Holzwarth AR, Muller MG (1996) Biophys J 35:11820
10. Ziolek M, Pawlowicz N, Naskrecki R AD (2005) J Phys Chem B 109:18171–18176
11. Gust D, Moore TA, Moore AL (1993) Acc Chem Res 26:1988
12. Gratzel M (1981) Acc Chem Res 14:376
13. Ballardini R, Balzani V, Credi A, Gandolfi MT, Venturi M (2001) Acc Chem Res 34:445
14. Gust D, Moore TA, Moore AL (2001) Acc Chem Res 34:40–48

15. Kodis G, Terazono Y, Liddell P, Andreasson J, Garg V, Hamburger M, Moore TA, Moore AL, Gust D (2006) J Am Chem Soc 128:1818–1827
16. Kestner NR, Logan J, Jortner J (1974) J PhysChem 78:2148–2166
17. Sumi H, Marcus RA (1986) J Chem Phys 84:4894–4914
18. Borrelli R, Di Donato M, Peluso A (2005) Biophys J 89: 830–841
19. Markel F, Ferris N, Gould I, Myers A (1992) J Am Chem Soc 114:6208–6219
20. Fischer SF, Van Duyne RP (1977) Chem Phys 26:9–16
21. Hopfield JJ (1974) Proc Natl Acad Sci USA 71:3640–3644
22. Duschinsky F (1937) Acta Phisicochim URSS 7:551–566
23. Sharp TE, Rosenstock KM (1964) J Chem Phys 41:3453–3463
24. Houghen JT, Watson JKG (1965) Can J Phys 43:298
25. Peluso A, Santoro F, Del Re G (1997) Int J Quant Chem 63:233–244
26. Doktorov EV, Malkin IA, Manko VI (1975) J Mol Spec 56: 1–20
27. Borrelli R, Peluso A, "MolFC: A program for Franck-Condon integrals calculation", 2004 Package available free of charge via Internet at http://pcdual.chem.unisa.it
28. Woodbury NWT, Becker N, Middendorf D, Parson WW (1985) Biochemistry 24:7516–7521
29. Kirmaier C, Holten D, Parson WW (1985) Biochim Biophys Acta 810:33–48
30. Gunner MR, Robertson DE, Dutton PL (1986) J Phys Chem 90:3783–3795
31. Gunner MR, Dutton LP (1989) J Am Chem Soc 111:3400–3412
32. McElroy JD, Mauzerall DC, Feher G (1974) Biochim Biophys Acta 333:261–278
33. Schenck CC, Parson WW, Holten D, Windsor MW, Sarai A (1981) Biophys J 36:479–489
34. Woodbury WT, Parson WW (1984) Biochim Biophys Acta 767:345–361
35. Franzen S, Boxer SG (1993) J Phys Chem 97:6304–6318
36. McPherson PH, Nagarajan V, Parson WW, Okamura MY, Feher G (1990) Biochim Biophys Acta 1019:91–94
37. Correa A, Di Donato M, Peluso A (2003) Chem Phys Lett 369:549
38. Breton J, Nabedryk E (1998) Photosynth Res 55:301–307
39. Brzezinsky B, Zundel G (1996) Faraday Discuss. 103:363
40. Zundel G (1992) Trends Phys Chem 3:129
41. Hung S, McPherson AN, Lin S, Liddell PA, Seely GR, Moore TA, Gust D (1995) J Am Chem Soc 117:1657–1658
42. Peluso A, Brahimi K, Carotenuto M, Del Re G (1998) J Phys Chem 102:10333
43. Del Re G, Brahimi M, Peluso A (1999) Chem Phys Lett 299:511
44. Peluso A, Di Donato M, Saracino GAA (2000) J Chem Phys 113:3212–3218
45. Okamura MY, Feher G (1992) Annu Rev Biochem 61:861
46. Kleinfeld D, Okamura MY, Feher G (1984) Biochemistry 23:5780–5786